Accelerated zinc oxide layers formation and their characterization

Bureš R., Jeníček J., Stoulil J.
Department of Metals and Corrosion Engineering, University of Chemistry and Technology Prague, Technická 5, 166 28 Prague, Czech Republic
E-mail: stoulilj@vscht.cz

This study investigates the formation of zinc oxide (ZnO) layers on zinc substrates under various environmental conditions and their characterization. Zinc samples were subjected to controlled exposure regimes including aqueous solutions and water vapour environments to stimulate the formation of ZnO. The resulting layers were characterized using X-ray diffraction (XRD), scanning electron microscopy (SEM/EDS), and optical microscopy. The analysis reveals correlations between exposure parameters and layer morphology, thickness, and phase composition. The study identifies key factors affecting ZnO layer quality and proposes pathways for optimizing these layers for potential sensing applications.

INTRODUCTION

Zinc oxide (ZnO) has attracted substantial attention due to its unique properties as a wide-bandgap semiconductor. Its applications span across photocatalysis, sensors, photovoltaics, and electroluminescent (EL) devices [1-4]. Nowadays, ZnO nanoparticles and nanostructures are examined preferably. To form this special nanosized ZnO, advanced processes have to be used [5-7]. On the contrary, ZnO can form naturally as a corrosion product on metallic zinc, which provides a low-cost and predictable route for its synthesis [8]. This study focuses on the controlled formation of ZnO layers on zinc substrates and evaluates their structure and composition.

ZnO exhibits a bandgap of ~3.37 eV and strong excitonic emission even at room temperature, making it suitable for ultraviolet and visible light emission [3, 9, 10]. ZnO crystals exhibit four dominant low-index surfaces: $(10\bar{1}0)$, $(11\bar{2}0)$, (0001), and $(000\bar{1})$. The last two are classified as polar surfaces, which play a key role in the material's applications and exhibit distinct chemical properties [11].

Natural oxidation of zinc in air or water leads to the formation of a thin ZnO layer. This process is driven by environmental factors such as humidity and temperature. For instance, zinc plates immersed in deionized water at ambient conditions form ZnO nanostructures over time, with initial agglomerates transforming into nanoflowers and microswords as immersion time increases [12]. Thermal oxidation involves heating zinc substrates in air or oxygen-rich environments to form ZnO layers. This method allows for precise control over the thickness and crystallinity of the oxide layer. For example, vacuum-deposited zinc thin films oxidized in hot water produce pencil-like nanorods, nanotubes, and lotus-like structures as oxidation time increases [13]. The pH of the solution and the concentration of precursors can also significantly influence the formation of ZnO nanostructures. Alkaline solutions with higher pH values tend to promote the growth of ZnO nanorods and nanosheets, while lower pH values may result in more compact or disordered structures [14, 15]. Understanding these conditions is crucial for tuning ZnO layer properties.

EXPERIMENTAL

Zinc samples (dimensions 20 × 10 × 1 mm) were prepared from zinc sheet and mechanically polished using P600 grit sandpaper. Fourteen specimens were exposed to seven different regimes (see Tab. 1).

For conditions 1-4, samples were fully immersed in the corresponding solution. In cases 5 and 6, samples were contaminated by immersion in 0.01 M NaCl and suspended above the liquid surface to simulate atmospheric corrosion. Exposure duration was 14 days except for regime 7 (ATM 300). Post-exposure, samples were rinsed with distilled water and ethanol, dried by warm air, and stored in PE bags.

Tab. 1 Exposures

No.	Regime	Name
1	Demineralized water at 70 °C	DEMI70
2	Demineralized water at 90 °C	DEMI90
3	0.01 M NaCl in demineralized water at 70 °C	NaCl70
4	0.01 M NaCl in demineralized water at 90 °C	NaCl90
5	Demineralized water at 70 °C (contaminated samples suspended above the solution)	ATM
6	Demineralized water at 70 °C (contaminated samples daily dried 1 hour at 70 °C, then re-exposed)	ATMCYCL
7	Atmospheric condition at 300 °C – 15 hours exposure	ATM300

Surface analysis was performed using X-ray diffraction (XRD, X'Pert Pro, PANalytical, EA Almelo, Holland) to identify crystalline phases, scanning electron microscopy with energy dispersive spectroscopy (SEM/EDS, VEGA3 LMU, TESCAN, Czech Republic/ OXFORD Instruments INCA 350, Great Britain) for surface morphology observation with elemental composition analysis, and optical microscopy on metallographic cross-sections prepared using standard grinding and polishing techniques. Metallographic cross-section was observed with an optical microscope (Olympus PME3, Japan).

RESULTS

Layer composition

XRD patterns confirmed the presence of ZnO as the dominant phase on samples exposed to elevated temperatures of 70 °C. Samples treated at 300 °C in a drying oven (ED 23, Binder, Germany) exhibited only a strong signal from the zinc substrate due to a very thin oxide layer. Other phases, such as chloride and basic zinc carbonates, formed probably by reactions with solutions, exhibited only a poor signal. Zinc silicate was detected only at elevated temperature of 90 °C. It could be an effect of the dissolution of the glass cell. The compositional results are summarised in Tab. 2.

Layer morphology

SEM imaging revealed significant differences in surface morphology based on exposure conditions. All images are summarized in Fig. 1.

A continuous and relatively homogeneous layer was observed after exposure in demineralized water at 70 °C, displaying a generally smooth surface with occasional localized porosity (Fig. 1a). This morphology suggests improved coverage of the underlying metal compared to the layers formed under other exposure conditions.

Exposure in demineralized water at 90 °C produced a notably more heterogeneous structure, featuring elongated, partially disrupted formations embedded within a relatively uniform flat surface, scattered with small spherical features (Fig. 1b). The visual appearance suggests reduced effectiveness in covering the metallic substrate, as indicated by distinct linear marks likely resulting from prior grinding.

Sample exposed in 0.01 M NaCl, 70 °C featured a surface morphology similar to that of the DEMI70 sample but exhibited greater heterogeneity due to the presence of flaky, poorly adherent spherical structures (Fig. 1c). These inhomogeneities may have locally exposed the underlying metal. Linear features, likely remnants of mechanical grinding, were again observed – though less frequently than in the previous sample – suggesting inferior surface coverage compared to DEMI70.

Tab. 2 XRD results, normalized to 100 % without Zn

No.	Exposure	Name	ZnO (%)	Contaminants
1	DEMI, 70 °C	DEMI70	100	zinc carbonate ($ZnCO_3$)
2	DEMI, 90 °C	DEMI90	16	84 % zinc silicate ($ZnSiO_3$)
3	NaCl, 70 °C	NaCl70	100	zinc chloride (ZnCl)
4	NaCl, 90 °C	NaCl90	85	11 % zinc silicate ($ZnSiO_3$) and 4 % zinc chloride (ZnCl)
5	DEMI, 70 °C, + NaCl contamination	ATM	100	
6	DEMI, 70 °C, + NaCl contamination with cyclic drying	ATMCYCL	100	zinc carbonate ($ZnCO_3$)
7	300 °C – 15 hours exposure	ATM300	too thin formed layer	

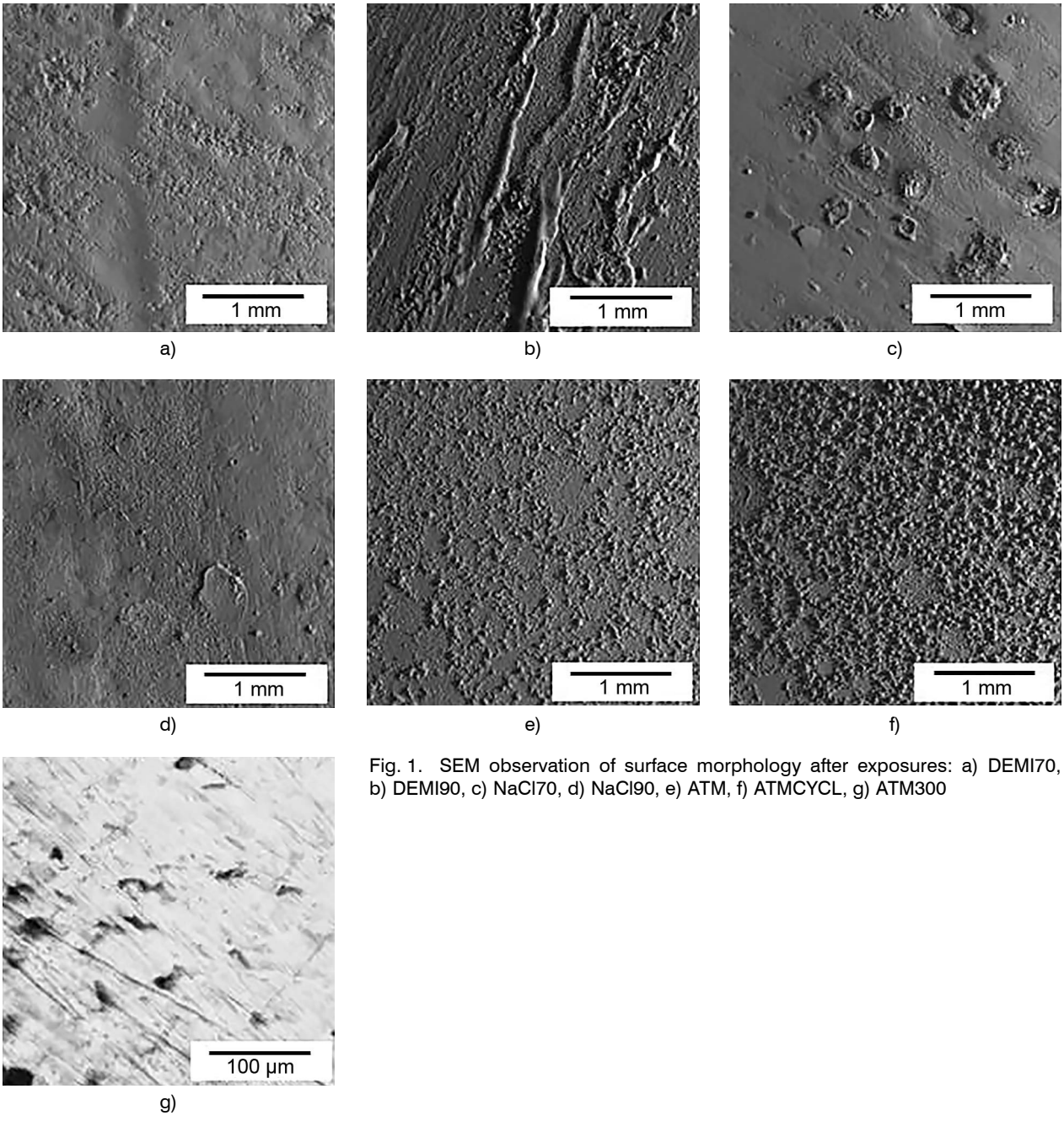

Fig. 1. SEM observation of surface morphology after exposures: a) DEMI70, b) DEMI90, c) NaCl70, d) NaCl90, e) ATM, f) ATMCYCL, g) ATM300

A combination of flaky, non-adherent spherical formations and smaller spherical particles characterizes the layer formed during the exposure in 0.01 M NaCl at 90 °C (Fig. 1d). These features are embedded in an otherwise continuous and homogeneous surface, where visible linear grooves – likely remnants of surface grinding – suggest incomplete metal coverage.

Corrosion products formed in water vapor at 70 °C after surface contamination with 0.01 M NaCl appeared as discontinuous crusts set within a flat surface marked by the highest density of sharp grooves observed among all samples (Fig. 1e). This morphology indicates the poorest coverage of the metal substrate in the study.

The surface sample morphology, at demineralized water vapor, 90 °C and 0.01 M NaCl surface contamination with cyclic drying regime, resembled the previous one but appeared slightly more covered, though still less so than other earlier samples (DEMI70, DEMI90, NaCl70, NaCl90, and ATM) (Fig. 1f). Compared to the ATM sample, the grooves were fewer and less pronounced, suggesting slightly improved metal coverage.

SEM observation of the sample surface exposed at 300 °C for 15 hours did not provide any relevant information, probably due to the small thickness of the layer (Fig. 1g). The presence of oxide on the surface was confirmed by EDS analysis.

Layer cross-section

Demineralized water at 70 °C

DEMI70 exposed by immersion in demineralised water at 70 °C was selected as the sample with the layer that best met the requirements for homogeneity, cohesion and coverage of the metal core. Cross-sectional analysis showed oxide layer thickness ranging from hundreds of nanometers to several micrometers. Under a light microscope in dark-field mode, a non-uniform layer of variable thickness was observed adjacent to the metal core (Fig. 2). In places, it was interrupted by voids or disturbed to expose metal (Fig. 3).

At a magnification of 1000× (Fig. 4), two distinct, sequentially layered structures were discernible on the zinc substrate. The layer directly adjacent to the metal appeared thinner and brighter in the BSE image compared to the overlying layer. EDS mapping across all examined regions (Fig. 4 and 5) revealed the highest oxygen concentration in the layer directly bonded to the metal. As expected, the strongest zinc signal originated from the metallic substrate, with a weaker response from the corrosion layers, although the inner layer produced a more pronounced signal than the outer one. Carbon was primarily concentrated in the outer layer and was most abundant in the embedding resin.

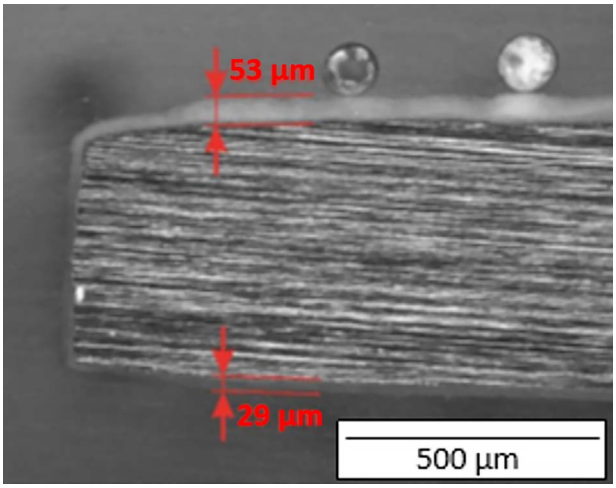

Fig. 2. DEMI, 70 °C, measured thickness of layer – 53 µm, 29 µm

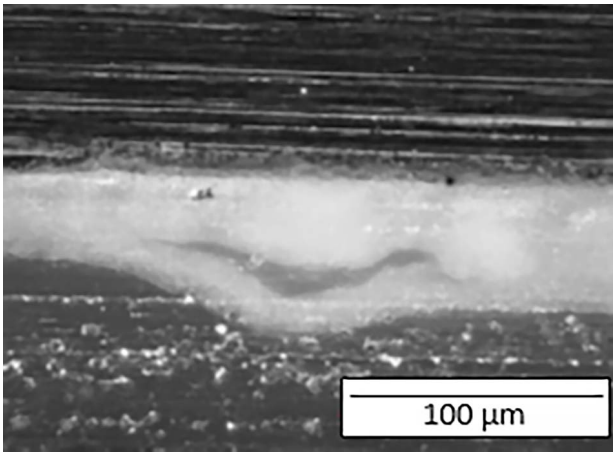

Fig. 3. A typical defect observed in the ZnO layer after exposure to DEMI water at 70 °C.

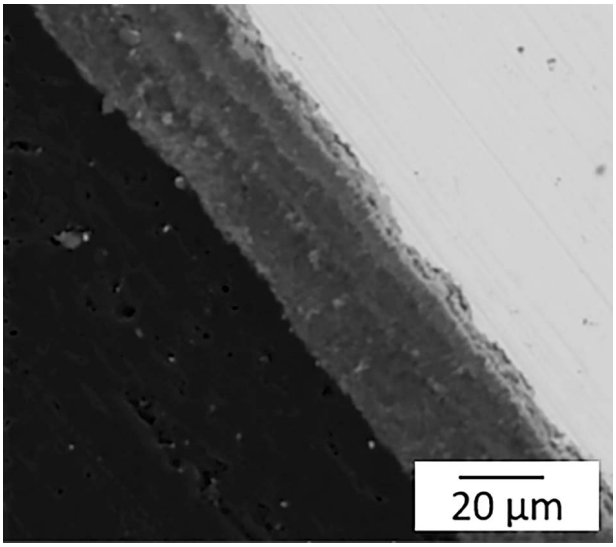

a)

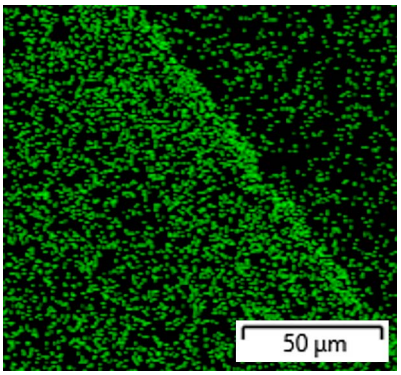

b) O Kα1

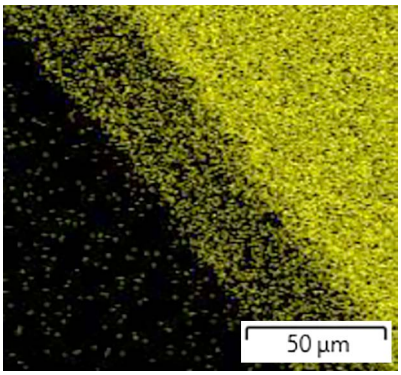

c) Zn Kα1

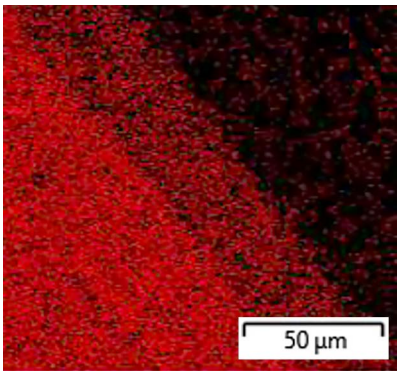

d) C Kα1_2

Fig. 4. SEM observation of a cross-section (a) and EDS mapping across the layer confirm the presence of oxygen (b), zinc (c), and carbon (d) in the ZnO layer (this is in agreement with the results from the XRD analysis)

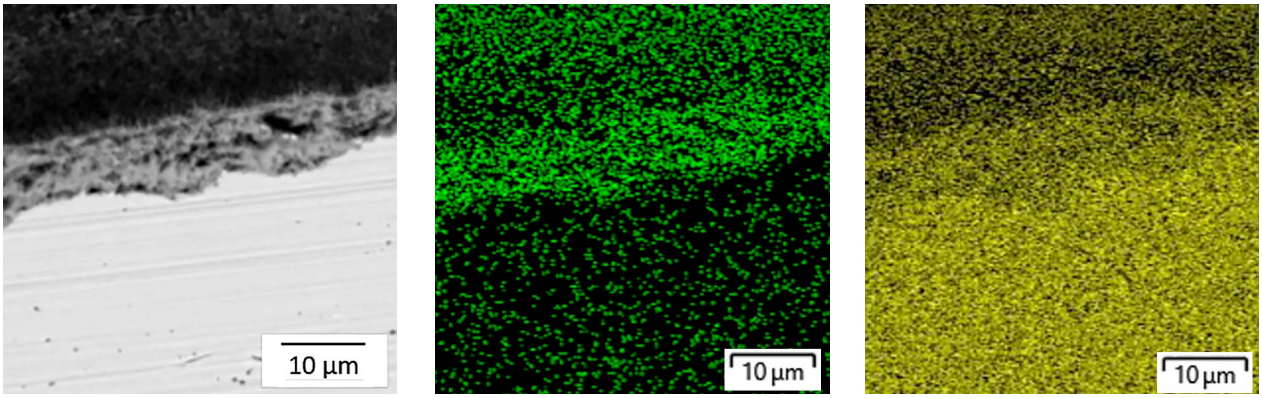

a) b) O Kα1 c) Zn Kα1

Fig. 5. EDS results revealed an inner layer exhibiting increased oxygen levels

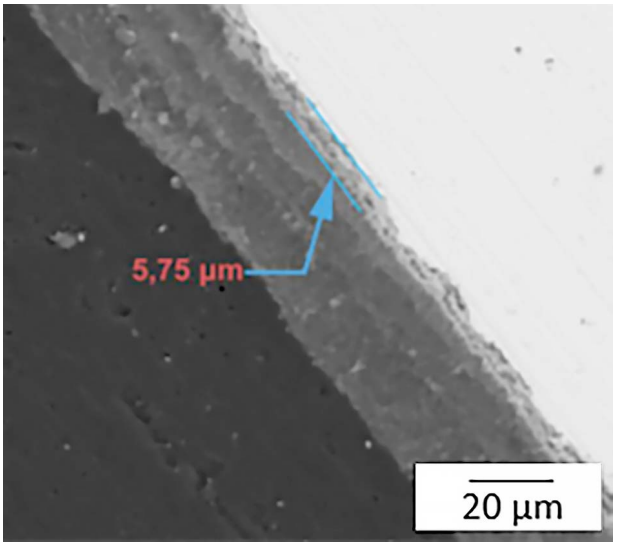

Fig. 6. Measurement of the thickness of the layer with increased oxygen content (5.75 µm)

The thickness of the aforementioned layer closely adhering to the metal and corresponding to ZnO according to the EDS results is approximately 5.75 µm as measured in the graphical (Fig. 6) editor.

Atmospheric condition at 300 °C – 15 hours exposure

As expected, the thin ZnO layer was not distinguishable under optical microscopy, and it was therefore documented exclusively using SEM. Fig. 7 shows an oblique cross-section of sample ATM300, revealing a barely visible, discontinuous surface layer on the metal, located on the right side of the image. The sample plane formed an angle of 12° with the observation plane, and thickness measurements obtained from the inclined cross-section were recalculated to represent perpendicular thicknesses using Equation 1. Measured thickness of 420 nm corresponds to 87 nm, and 360 nm to 75 nm in the perpendicular section.

$$a = c \cdot \sin \alpha \qquad (1)$$

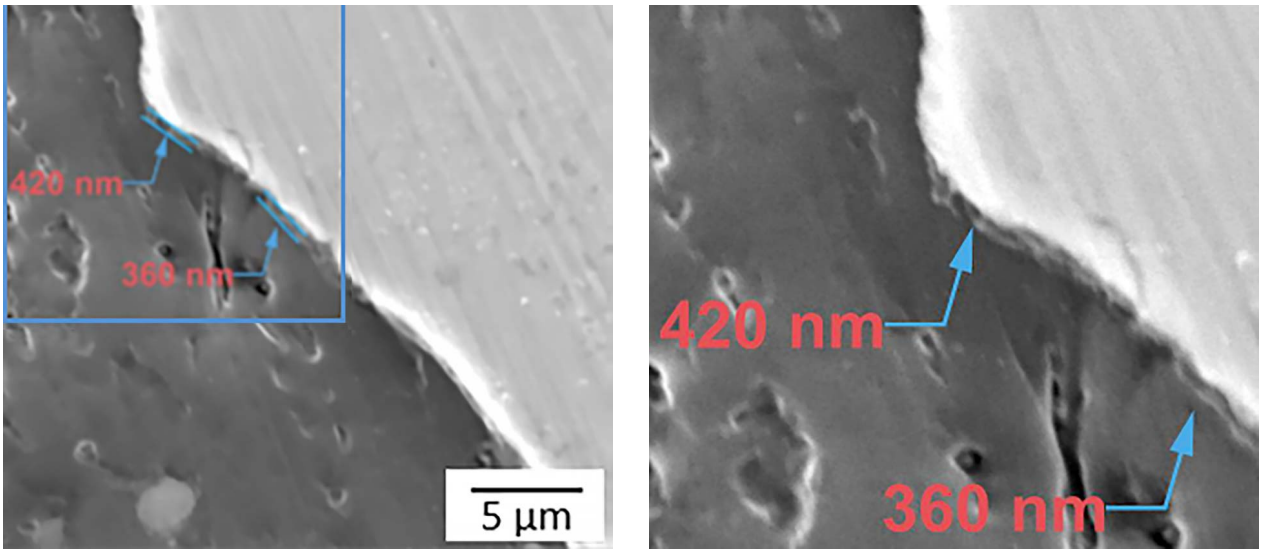

a) b)

Fig. 7. Cross-sectional measurement of the ZnO layer (420 nm, 360 nm) after 15 hours exposure at 300 °C (a), detail in (b)

DISCUSSION

The experimental investigation clearly demonstrated that the nature of the exposure environment – particularly temperature, solution composition, and physical state (liquid vs. vapor) – significantly influenced the structure, thickness, and phase composition of the corrosion layers formed on zinc surfaces. XRD analysis revealed that ZnO was the dominant corrosion product in nearly all exposure regimes, though its purity and crystallinity varied. The DEMI70 sample in particular developed a highly compact and homogeneous ZnO layer. SEM analysis supported the phase findings by showing marked differences in surface morphology. The DEMI70 sample exhibited the most continuous and uniform ZnO layer, correlating with effective metal coverage. In contrast, samples exposed to water vapor environments (ATM and ATMCYCL) formed discontinuous crust-like layers, with prominent surface scratches and minimal coverage of the metal. While cyclic drying (ATMCYCL) offered marginal improvement in layer compactness, these regimes still resulted in the least effective protective performance overall. Cross-sectional analysis of the DEMI70 sample revealed a bilayer structure, with an inner ZnO-rich layer of approximately 5.75 μm thickness and an outer, more carbon-rich layer. The presence of carbon in the outer zone, in conjunction with XRD results, suggests the partial formation of basic zinc carbonate, likely due to limited CO_2 ingress during or after exposure. The thin ZnO film formed at 300 °C was observable only via SEM and consisted of a discontinuous layer barely distinguishable from the metallic substrate.

CONCLUSIONS

The exposure regime using demineralized water at 70 °C (DEMI70) produced one of the most compact and homogeneous ZnO layers, offering the most effective metal coverage among all tested conditions. Metallographic analysis showed an inner layer, approximately 6 μm thick, composed primarily of zinc and oxygen, indicating a predominance of ZnO. The outer layer contained lower levels of zinc and oxygen, but higher carbon content, suggesting partial presence of zinc carbonate, also indicated by XRD analysis. In comparison, thermal oxidation of zinc at 300 °C in air yielded a significantly thinner ZnO layer (tens of nanometers, based on SEM) but was obtained through a simpler preparation method.

Acknowledgement

A financial support of the grant LUC23160 of InterExcellence II – Ministry of Education, Youth and Sports is gratefully acknowledged.

REFERENCES

1. Könenkamp, R., R.C. Word, and M. Godinez, Ultraviolet Electroluminescence from ZnO/Polymer Heterojunction Light-Emitting Diodes. *Nano Letters*, **2005**. 5(10): p. 2005-2008.
2. Lim, J.-H., et al., UV Electroluminescence Emission from ZnO Light-Emitting Diodes Grown by High-Temperature Radiofrequency Sputtering. *Advanced Materials*, **2006**. 18(20): p. 2720-2724.
3. Tan, S.T., et al., Ultraviolet and visible electroluminescence from n-ZnO⁄SiOx⁄(n,p)-Si heterostructured light-emitting diodes. *Applied Physics Letters*, **2008**. 93(1).
4. Zhong Lin, W., Zinc oxide nanostructures: growth, properties and applications. *Journal of Physics: Condensed Matter*, **2004**. 16(25): p. R829.
5. Hong, R., et al., Synthesis and surface modification of ZnO nanoparticles. *Chemical Engineering Journal*, **2006**. 119(2): p. 71-81.
6. Lauritsen, J.V., et al., Stabilization Principles for Polar Surfaces of ZnO. *ACS Nano*, **2011**. 5(7): p. 5987-5994.
7. Wu, H., et al., Controlled growth of uniform two-dimensional ZnO overlayers on Au(111) and surface hydroxylation. *Nano Research*, **2019**. 12(9): p. 2348-2354.
8. Goodwin, F.E., *3.13 - Corrosion of Zinc and its Alloys**, in *Shreir's Corrosion*, B. Cottis, et al., Editors. 2010, Elsevier: Oxford. p. 2078-2093.
9. Batyrev, E.D. and J.C. van den Heuvel, Modification of the ZnO(0001)–Zn surface under reducing conditions. *Physical Chemistry Chemical Physics*, **2011**. 13(28): p. 13127-13134.
10. Claeyssens, F., et al., Growth of ZnO thin films – experiment and theory. *Journal of Materials Chemistry*, **2005**. 15(1): p. 139-148.
11. Mora-Fonz, D., et al., Why are polar surfaces of ZnO stable? *Chemistry of Materials*, **2017**. 29(12): p. 5306-5320.
12. Criado, D., A. Zúñiga, and A. Pepinelli, Green, Water-Based Synthesis of ZnO Nanostructures. *Journal of the Brazilian Chemical Society*, **2023**. 35.
13. Balela, M.D.L., et al., Formation of zinc oxide nanostructures by wet oxidation of vacuum deposited Zn thin film. *Optical and Quantum Electronics*, **2016**. 49(1): p. 3.
14. Ainuddin, A. and W.N.A.M. Idris, Growth of ZnO nanostructures with different alkaline precursor solution. **2016**. 11: p. 7612-7616.
15. LU, P. and D. XUE, selective synthesis of ZnO arrays. *Surface Review and Letters*, **2010**. 17(02): p. 261-264.